Toward printable solar cells based on PbX colloidal quantum dot inks

Yang Liu, Guozheng Shi, Zeke Liu [ID]* and Wanli Ma [ID]*

Lead chalcogenide (PbX, X = S, Se) colloidal quantum dots (CQDs) are promising solution-processed semiconductor materials for the construction of low-cost, large-area, and flexible solar cells. The properties of CQDs endow them with advantages in semi-conducting film deposition compared to other solution-processed photovoltaic materials, which is critical for the fabrication of efficient large-area solar cells towards industrialization. However, the development of large-area CQD solar cells is impeded by the conventional solid-state ligand exchange process, where the tedious processing with high expense is indispensable to facilitate charge transport of CQD films for photovoltaic applications. In the past several years, the rapid development of CQD inks has boosted the device performance and dramatically simplified the fabrication process. The CQD inks are compatible with most of the industrialized printing techniques, demonstrating potential in fabricating solar modules for commercialization. This article aims to review the recent advances in solar cells based on PbX CQD inks, including both lab-scale and large-area photovoltaic devices prepared from solution-phase ligand exchange (SPLE) as well as the recently invented ''one-step'' synthesis. We expect to draw attention to the enormous potential of CQD inks for developing high-efficiency and low-cost large-area photovoltaics.

1. Introduction

Solution-processed solar cells have received tremendous attention due to their low cost, scalable manufacturing and mechanical flexibility. These advantages can potentially reduce the production costs to a competitive level against the mainstream PV markets. Metal halide perovskites, semiconducting organics and colloidal quantum dots (CQDs) are currently the three primary classes of solution-processed photovoltaic materials.[1] The solar cells built from these materials could be constructed at low temperature (<200 °C) through various deposition techniques (spin coating, spray coating, blade coating, inkjet printing, *etc.*) on both rigid and plastic substrates. Up to now, the certified power conversion efficiency (PCE) of single-junction

Jiangsu Key Laboratory for Carbon-Based Functional Materials & Devices, Institute of Functional Nano & Soft Materials (FUNSOM), Soochow University, 199 Ren-Ai Road, Suzhou Industrial Park, Suzhou, 215123 Jiangsu, P. R. China. E-mail: zkliu@suda.edu.cn, wlma@suda.edu.cn

Yang Liu is currently a Master's student under the supervision of Prof. Wanli Ma at Soochow University. He obtained his BS.degree from Anhui Agricultural University. His current research interest focuses on the direct synthesis of PbX quantum dot inks and their application in optoelectronic devices.

Yang Liu

Guozheng Shi is currently a postdoctoral scholar at Soochow University. He obtained his PhD degree in Material Science from the Institute of Functional Nano & Soft Materials (FUNSOM) at Soochow University under the supervision of Prof. Wanli Ma in 2019. During his PhD study, he worked at Graduate School of Energy Science, Kyoto University as a joint PhD student with Prof. Takashi Sagawa. His current research interest focuses on the printable quantum dot solar cells.

Guozheng Shi

solar cells based on these materials has reached 25.2% (perovskites), 17.4% (organics) and 16.6% (CQDs), respectively.[2]

It is worth noting that these high efficiencies are all achieved by lab-scale devices with active areas of ~ 0.1 cm^2. For commercialization, it is necessary to achieve high PCEs on large-area (>800 cm^2) solar modules, which, however, is still challenging. For example, the performance of perovskite solar cells highly relies on the crystallization process during film depostion.[3] A film with larger crystalline grains and denser morphology normally exhibits higher device performance.[4] However, it is difficult to control the sophisticated crystallization process in scale-up manufacturing. So far, the highest National Renewable Energy Laboratory (NREL) certified PCE of a perovskite small module is only 17.9%.[5] This is analogous to the scale-up of organic solar cells. Limited by the short diffusion length of organic materials, the phase separation between donors and acceptors requires good manipulation to construct a bulk-heterojunction network for efficient charge separation and transport.[6] This process becomes more challenging for large-area film deposition. In contrast, CQDs, especially lead chalcogenides (PbX, X = S, Se), may be more suitable as building blocks for efficient, large-area and low-cost solar cells owing to their unique properties.

(1) Excellent stability. PbX CQDs possess a simple composition with an exclusively stable crystal structure of cubic rock-salt, resulting in facile synthesis and high material stability (Fig. 1a and b). Through careful surface engineering, halogens could work as an effective passivant on CQD surfaces, and protect them from being attacked by the aggressive ambient oxygen.[7] The PbS CQD solar cells without any encapsulation exhibit excellent air- and photo-stability, retaining steady PCEs in air for half to four years (Fig. 1c),[8,9] which is at the highest level among all solution-processed solar cells. Moreover, the remarkable air-stability indicates that the whole film deposition process can be conducted under ambient conditions, facilitating low-cost mass-manufacturing.

(2) Facile film deposition. As one of the most strongly quantum confined materials, the close-packed PbX CQDs possess high inter-dot coupling energy of excitons, which is comparable to the exciton binding energy (100 meV). This allows significant elongation of the electronic wave function out of CQDs, endowing exciton dissociation in PbX CQD films at room temperature (Fig. 1d).[10] As a result, charge separation and transport could be easily realized in CQD solids, without the need of donor/accept interfaces as in organic solar cells or the high-temperature sintering as in CdTe CQDs solar cells.[11] Meanwhile, the CQDs are already highly crystalline, so the sophisticated crystallization control is not required during film formation, while it is pivotal for the deposition of perovskite thin films. Thus, the decoupling of the crystallization process from film deposition can greatly simplify the morphology control of large-area devices, and makes CQD solids an excellent candidate for scale-up manufacturing of solution-processed solar cells (Fig. 1e).

(3) Low cost ink. Substantial advances in PbX CQD inks have been achieved in a recently developed direct-synthesis method.[12] The materials cost for the PbX CQD ink has been reduced to lower than 5 \$ g^{-1}, making CQD solar cells possibly competitive against the cost of perovskite solar cells.[13] In contrast, the current materials cost for organic photovoltaic semiconductors can be very expensive, up to several hundred dollars per gram.[14]

To realize the practical application of PbX CQD solar cells, efficient QD ligand management has to be developed. The surface ligands of long alkyl chains endow NCs with controllable size distribution and solution processability, but, however, they have to be exchanged by short ones to transform NC solids into the semi-conducting arrays for optoelectronic applications. Unfortunately, compressive stress induced by ligand exchange processing results in detrimental cracks in the NC film. To improve film quality, repeated layer-by-layer (LbL) deposition processing (~ 5–10 times) is indispensable, which, however,

Zeke Liu is an associate professor at Soochow University. He obtained his PhD degree from Soochow University under the supervision of Prof. Shuit-Tong Lee in 2016. During his PhD study, he worked at Lawrence Berkeley national laboratory as a joint PhD student with Prof. Paul Alivisatos. Before he joined Soochow University in 2019, he worked as a joint postdoctoral scholar in Prof. Wanli Ma's group at Soochow University and Prof. Xingchen Ye' group at Indiana University Bloomington. His current research interest focuses on the design/synthesis of nanocrystals and their application in optoelectronic devices.

Zeke Liu

Wanli Ma is currently a professor in the Institute of Functional Nano & Soft Materials (FUNSOM) at Soochow University. He received his PhD degree in 2006 from the University of California at Santa Barbara under the supervision of Prof. Alan J. Heeger. Before he joined Soochow University in 2010, he worked as a postdoctoral scholar in Prof. Paul Alivisatos' group at Lawrence Berkeley national laboratory. His publications have been cited over 18 000 times. His current research interest focuses on developing solution-processed solar cells, including nanocrystals, organic materials and perovskite.

Wanli Ma

Fig. 1 (a) Typical transmission electron microscopy (TEM) images of PbS CQDs. The inset shows the crystal structure of PbX. (b) High-resolution TEM image of a single PbS QD. Reprinted with permission from ref. 23. Copyright 2014, American Chemical Society. (c) The air-stability (top) and photo-stability (bottom) of PbS CQD solar cells in air ambient. Reprinted with permission from ref. 8. Copyright 2014, Nature Publishing Group (top). Reprinted with permission from ref. 24. Copyright 2019, Nature Publishing Group (bottom). (d) Schematic description of the effect of quantum confinement effect on exciton dissociation in coupled CQD assembles. For QDs with strong quantum confinement effect/large exciton Bohr radius (e.g. PbX), the inter-NC coupling energy between the QDs is comparable with their exciton binding energy, which enables the excitons to dissociate without the aid of an external potential gradient. Whereas, the exciton recombination is preferable for the QDs that assemble with a small exciton Bohr radius (e.g. CdX). (e) The solution-phase synthesis of PbX CQDs is compatible with all industrial deposition techniques. Reprinted with permission from ref. 25 Copyright 2012, Nature Publishing Group. (f) Efficiency progress of PbS CQD solar cells.

increases the manufacturing complexity and cost (Fig. 2 top).[15,16] This tedious fabrication process will certainly impede the exploration of large-area solar cells based on PbX CQDs. To resolve this challenge, CQD inks with inorganic surface ligands have been developed, which can be directly coated on the substrates using a single deposition step to achieve semiconducting large-area films. After having been developed for almost a decade, fruitful progress has been achieved in solar cells employing CQD inks. Especially in 2017, Prof. Sargent's group reported a high-performance photovoltaic device using PbS CQD inks, benefiting from the improved solution-phase ligand exchange processing.[17] This work ignited a new round of research efforts on PbX CQD solar cells and boosted the highest PCE further to 13.8%,[18] exceeding the record PCE of

11.8% for the device based on solid-state ligand exchange (Fig. 1f).[19] Recently, we proposed a more advanced "one-step" strategy to directly synthesize PbS CQD inks, which could significantly simplify the preparation of the materials and reduce the related cost.[12] Besides, this scalable synthesis is compatible with mass-manufacturing. It is worth noting that most previous reviews on PbX solar cells are mainly focused on conventional solid-state ligand exchange.[20–22] The rapid progress of PbX CQD inks in recent years can provide new opportunities for large-area photovoltaics in the near future, which haven't yet been seriously addressed.

In this mini-review, we summarize the recent progress in solar cells based on PbX CQD inks toward large-area photovoltaic

Fig. 2 Schematic representation of semi-conducting PbX CQD films prepared based on solid-state ligand exchange (top) and solution-phase ligand exchange (bottom). Reprinted with permission from ref. 12. Copyright 2019, Nature Publishing Group.

applications. First, the progress in PbX CQD solar cells based on solution-phase ligand exchange, a widely applied strategy to acquire PbX CQD inks, will be discussed. Then, we will introduce the insights into the recently developed direct-synthesis technique for CQD inks, which is promising for low-cost mass manufacturing. Furthermore, the explorations of large-area PbX CQD solar cells will also be reviewed. Finally, further challenges and perspectives towards large-area PbX CQD solar cells will be proposed.

2. PbX CQD solar cells based on solution–phase ligand exchange (SPLE)

In a typical SPLE process (Fig. 2 bottom), the PbX CQDs dissolved in hexane or octane are added to polar *N,N*-dimethylformamide (DMF) containing different short or atomic ligands (thiols, lead halides, *etc.*). After being mixed vigorously, the PbX CQDs are transferred from the top oil phase to the bottom polar phase. During the phase transformation, the long alkyl chain ligands on CQD surfaces, that could sterically stabilize CQDs in nonpolar solvents, are exchanged to charged ions, screening individual CQDs in the protic solvents with high dielectric constant. The CQDs are then purified and re-dispersed in solvents (DMF, butylamine, *etc.*) for film deposition. Compared to the conventional solid-state ligand exchange, the SPLE can not only simplify the fabrication process but also ensure more uniform ligand exchange, and hence reduces the band-tails, which further boosts the device performance.[17] Up to now, CQD solar cells with PCE > 12% have all employed this strategy. Nevertheless, there is still room to optimize the passivation in the regime of SPLE. Throughout the history of PbX CQD solar cells, the exploitation of efficient passivation of CQD inks is the dominant overarching theme to promote the progress of this field. Notably, the strategy of SPLE ignited the development of IR solar cells based on low-bandgap/large-size CQDs, which show potential in tandem solar cells as the ideal complement in absorption spectra with that of perovskites or silicon. In this section, we will review the development of solar cells based on both small and large size PbX CQDs employing SPLE.

2.1. PbX solar cells based on near-infrared-bandgap (small size) CQD inks

The concept of SPLE can be traced back to polymer/Cd chalcogenide (CdX, X = S, Se, Te) nanocrystal (NC) hybrid solar cells, in which the CdX NCs were firstly treated with pyridine to exchange the insulating native ligands and facilitate charge transfer before mixing with polymer.[26,27] This method was then applied in PbS CQD solar cells by exchanging the native ligands with octylamine or butylamine.[28,29] However, these alkylamines are still too long to ensure efficient charge transport. Inspired by the decent performance of CQD devices based on solid-state ligand exchange employing thiols ligands, coupled thiol ligands were used to ligand exchange PbS CQDs in solution.[30,31] However, the photovoltaic performance based on these inks was deficient (~2%) due to the unsatisfactory surface passivation, reflected from the largely reduced photoluminescence quantum

yield (PLQY).[30] In 2014, Dirin *et al.* introduced perovskite and metal halide complexes as inorganic capping ligands for PbS CQDs.[32] The MAPbI$_3$ capped PbS CQD inks can retain almost the same PLQY as the original CQDs capped with oleic acid (OA), indicating excellent passivation. This may be attributed to the atomic-scale crystalline coherence between the two materials and the formation of type-I band structure.[33] Soon Ning *et al.* used MAI as the capping ligand to exchange the original OA, obtaining a photovoltaic device with a PCE of 6.1%.[34] In this work, the butylamine (BA) was suggested as an effective solvent to disperse the PbS CQD inks, since BA can bind on PbS QD surfaces weakly and support dispersibility for the QDs. Furthermore, BA possesses a low boiling point (78 °C), and can be easily removed during film deposition. Therefore, BA has been widely used as the solvent for the SPLE PbS QD inks to date. In 2015, perovskite precursor solution (MAI + PbI$_2$) was used to exchange PbS CQDs.[35] By combing this insightful passivation method with improved device structure, a PCE approaching 9% was achieved. Then various preparation methods of CQD inks have been extensively reported.[36,37] However, all devices based on CQD inks exhibited a relatively lower performance compared to those prepared through LbL solid-state ligand exchange processing, until 2017, when Liu *et al.* developed a (PbI$_2$ + PbBr$_2$ + NH$_4$Ac) protocol (Fig. 3a).[17] The exchanged PbS CQDs exhibit sharper band edge compared to those prepared by MAPbI$_3$ SPLE or TBAI solid-state ligand exchange. As a result, a certified PCE of 11.3% was achieved with decent device stability. The unencapsulated devices could keep stable in air for over 1000 hours. The PCE of CQD-ink-based solar cells has exceeded that of those fabricated by solid-state ligand exchange for the first time. Meanwhile, Aqoma *et al.* also independently reported a similar SPLE method using only PbI$_2$ as the ligand precursor, leading to a PCE of 10.15%.[38] Zhang *et al.* conducted a detailed investigation to compare the difference of PbS QD solid based on SPLE and SSLE from soft and hard X-ray photoelectron spectroscopy characterization and the related device physics study.[39] It was concluded that the better photovoltaic performance of the SPLX-based solar cell is attributed to a combination of higher built-in potential, lower trap density in the CQD solid, and interference effects due to a smoother film surface. A further improvement of the PCEs up to 11.6% was achieved by subsequent fine optimization of the Pb precursor,[40] ammonium salts,[41] and electron transport layer.[42] In 2018, Xu *et al.* developed new ink solvents involving mixed amines (butylamine, amylamine and hexylamine) instead of the sole butylamine reported previously. A 2D matrix of PbI$_2$–amine complexes can be formed around PbS CQDs, which can reduce the structural and energetic disorder in PbS CQD films (Fig. 3b–d).[43] The concomitantly improved photocarrier diffusion length afforded efficient charge transport in the CQD film with an increased optimal thickness up to ~600 nm. The photovoltaic device shows a champion PCE of 12.48% and a certified PCE of 12.01%. In addition to MAPbI$_3$ and Pb halogen salts, all inorganic CsPbI$_3$ and triple-cation (CsMAFA) perovskites were also explored to coat on PbS CQDs *via* SPLE.[44,45] Moreover, a preferable lattice matching between PbX CQDs and CsPbBr$_x$I$_{1-x}$ perovskites was found, which prevents oxidation of the CQD surfaces and reduces
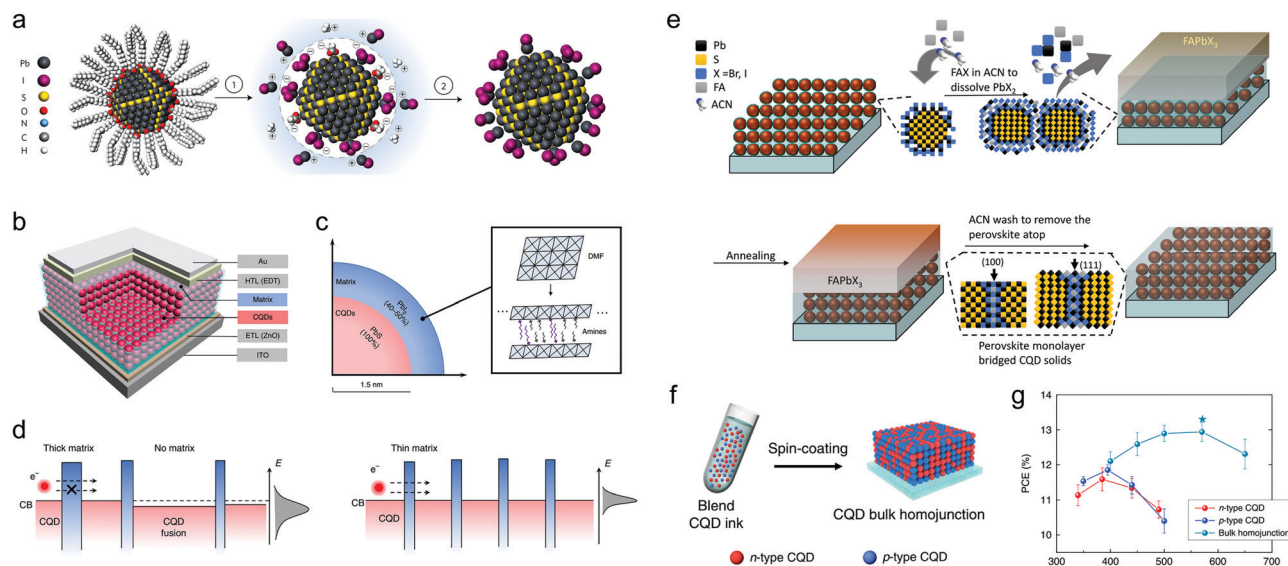
Fig. 3 (a) Solution-phase ligand exchange with metal halide precursors and ammonium acetate. Process 1 (ligand exchange): the bulky oleic acid ligands are replaced by the [PbX$_3$]$^-$ anions with the aid of ammonium protons. The CQD surface is stabilized by both [PbX]$^+$ and [NH$_4$]$^+$. Process 2 (CQD precipitation): after ligand exchange, CQDs are precipitated *via* the addition of toluene, an anti-solvent, and are separated by centrifugation. Reprinted with permission from ref. 17. Copyright 2017, Nature Publishing Group. (b) Schematic diagram of the effective medium model of the CQD absorber in a solar cell, where CQDs (red) assemble in a matrix medium (blue). (c) The matrix consists of PbI$_2$, which is enough to account for the formation of full monolayer coverage on the surfaces of PbS CQDs (bandgap ~1.3 eV and diameter ~3 nm). The dimensional structure of the matrix can be tuned using solvents. (d) The schematic diagram for the effect of homogeneity of the matrix on the structural and energetic order of CQD film. Confining the matrix dimensionality between the CQDs and improving its homogeneity throughout the film can increase the photocarrier diffusion length and reduces the V_{oc} deficit. Reprinted with permission from ref. 43. Copyright 2018, Nature Publishing Group. (e) Schematic of the formation of monolayer perovskite bridges among the QDs. The perovskite matrix is formed first by soaking the pre-exchanged CQD films in a FAX (X = Br, I) solution, where the FAX solution dissolves the PbX$_3^-$ ligands and perovskite grows between adjacent PbS CQDs. The films are annealed and then washed with acetonitrile to remove excess perovskite. Reprinted with permission from ref. 18. Copyright 2014, Elsevier. (f) The bulk-homojunction films were fabricated by depositing the blended CQD inks comprising n-type and p-type CQDs. (g) Thickness-dependent PCE for bulk-homojunction devices and n-type CQD devices. Bulk-homojunction devices enable the use of much thicker CQD films compared with the case of n-type CQD devices, indicating the increase of carrier diffusion length. Reprinted with permission from ref. 49. Copyright 2020, Nature Publishing Group.

the CQD agglomeration. The PCE of the device employing this lattice-anchored strategy reached 12.6% with enhanced photostability.[24] The unencapsulated devices can retain 95% of their initial PCE following 2 h of continuous AM1.5G illumination, whereas the control device (exchanged with PbI$_2$ + PbBr$_2$ + NH$_4$Ac) degraded to 70% of their initial PCE value within an hour. It is worth mentioning that the incorporation of PbS CQDs into CsPbBr$_x$I$_{3-x}$ can also suppress the perovskite transition to δ-phase configuration, which is important for their optoelectronic applications. In addition to the composition of the perovskite matrix, the thickness control of the matrix is also pivotal to facilitate charge transport between QDs and maximize the device performance. Sun *et al.* recently developed a post-treatment strategy to form monolayer perovskite bridges among QDs, enabling the union of surface passivation with improved charge transport (Fig. 3e).[18] As a result, a doubled diffusion length was achieved compared to the reference CQD solids. The PCE was then improved to 13.8%, which is the highest efficiency for PbX CQD solar cells so far.

To fully utilize solar energy, compact CQD solids with a thickness of around 1 micrometer are required.[46] However, the serious trapping behavior and short diffusion length of CQD

solids limited the carrier collection in such a thick film.[47] To address this issue, two different kinds of inks were used together in PbX CQD solar cells to construct a bulk-homojunction. Yang *et al.* attempted to fabricate a CQD bulk-heterojunction by mixing MAPbI$_3$ capped PbS CQD ink (donor) with a thioglycerol (TG) capped one (acceptor).[48] Benefitting from the tightly bonded ligands, the properties of these two types of CQDs can be preserved in the uniformly mixed CQD film. By optimizing the D : A ratio, photocarriers can migrate efficiently through their respective donor/acceptor phase. However, the device performance was only 10.5%, possibly due to the unsatisfactory passivation of TG capped PbS CQDs. Recently, Choi *et al.* further optimized this bulk-homojunction through a cascade surface modification (CSM) strategy, in which a standard halogenation SPLE step was first conducted to form an n-type CQD ink with sufficient passivation. Then a subsequent step reprograms the CQD surfaces with cysteamine (CTA) to achieve a p-type PbS CQD ink. Meanwhile, the NH$_2$ group of CTA enabled the stable dispersion of the CQDs in butylamine.[49] As a result, the carrier diffusion length can reach 340 nm, which is 1.5-fold longer than that of the previously reported best CQD films (221 nm). Finally, a record PCE of 13.3% was achieved (Fig. 3f and g).

The development of SPLE realizes one-step deposition of the active layer in PbX CQD solar cells, which significantly simplified the overall fabrication process, whereas the hole transport layer (HTL) PbS-EDT (EDT capped PbS CQDs) still relies on LbL solid-state ligand exchange. To further achieve fully printable CQD solar cells *via* fast deposition, the PbS-EDT CQD layer needs to be replaced. Aqoma *et al.* reported a method for the preparation of p-type PbS CQD inks by SPLE with MPA. These p-type inks can disperse well in the mixed solvent of water and butylamine, which can be deposited on the underneath n-type PbS CQD film. This printable device exhibited comparable performance with the conventional device using PbS-EDT as the HTL.[50] It is worth noting that semiconducting organics have also been used as efficient HTLs in CQD solar cells based on the Schottky structure,[51,52] and homo-junction structure (ITO/polymer/PbS-EDT/PbS-TBAI/LiF/Al) with a PCE of 8.45%.[53] In 2018, Aqoma for the first time replaced the PbS-EDT layer with a p-type polymer (ITO/ZnO/PbS inks/PTB7/MoO$_x$/Ag) and obtained a PCE of 9.6%.[54] The PCE of this hybrid structure was then improved to 11.5% through molecular engineering of these organic polymers.[55,56] Zhang *et al.* further demonstrated multiple organic bulk-heterojunction films with PTB7-Th blending with various N-type acceptors can work as an efficient HTL in PbS solar cells, which is superior to the device with sole PTB7-Th as the HTL and results in a PCE exceeding 12%.[57] Baek *et al.* also incorporated small molecule bridges into the polymer layer that improved the near-infrared absorption and charge separation, leading to a maximum PCE of 13.1% with great stability at the maximum power point (MPP).[58]

PbSe possesses a larger Bohr radius (46 nm) compared to PbS (20 nm),[59] which leads to stronger electronic coupling and hence better charge carrier transport.[60] The effective confinement of PbSe CQDs gives rise to the multiple exciton generation (MEG) effect,[61,62] pushing the theoretical photovoltaic efficiency over the S–Q limit. However, the development of PbSe CQD solar cells lags significantly behind PbS ones due to their air instability and unsatisfactory surface passivation. *In situ* dual passivation was achieved by the cation exchange technique, which largely solved the stability issue.[63,64] By employing materials with the desired band-alignment, the PbSe solar cell efficiency has been improved to 9.2%.[65] Recently, Ahmad *et al.* and Hu *et al.* reported the application of the SPLE strategy in the fabrication of PbSe CQD solar cells independently. The improved surface passivation further boosted the PCE up to 10.65%.[66,67] This is the first time for PbSe CQD solar cells to achieve efficiency exceeding 10%, which also demonstrates the versatility of the SPLE strategy in different CQD systems. The solar cell performances based on small-size PbX CQD inks are listed in Table 1.

2.2. PbS solar cells based on infrared-bandgap (large size) CQD inks

The balance between voltage and current in solar cells necessitates the bandgap of photovoltaic materials in the range of 1.1–1.4 eV in a single-junction solar cell as referred to the S–Q limit, which inevitably leads to the waste of solar energy, *i.e.*, the transmittance loss of sub-bandgap-energy photons. For example, the crystalline silicon (c-Si) fails to absorb infrared (IR) photons

beyond 1100 nm, and perovskite can only absorb light with a wavelength less than ~900 nm (Fig. 4a). However, the infrared region accounts for almost half of the integrated solar spectrum. To minimize these energy losses, tandem structures can be employed in photovoltaic devices, in which a subcell with a narrow-bandgap material is stacked on the top of the subcell consisting of materials such as c-Si or perovskite. Among all solution-processed photovoltaic materials, PbX CQDs are the most suitable candidates as infrared absorbers, since their bandgap can be easily tuned to cover the spectrum from ~600 nm up to 4000 nm.[81] Thus, the IR solar cells based on large-size PbX CQDs have attracted substantial attention and developed rapidly in the past several years. Note that the "IR CQDs" are defined following the literature as the CQDs with an absorption peak over 1100 nm. To simulate additionally-added Si power points based on these IR CQDs, an 1100 nm long-pass filter or a silicon front cell was placed between the sample and AM1.5 solar simulator during J-V scanning. The acquired PCE was defined as the IR-PCE.[82,83]

The PbX CQDs surface consists of nonpolar {100} facet (Pb/X = 1) and polar Pb-terminated {111} facet. It was revealed that the shape of OA-capped PbS CQDs would transform from octahedron to cub-octahedron as size increases (Fig. 4b).[84] The optimal size for PbS CQDs used in single-junction solar cells is around 3 nm, which makes {111} the dominant surface facets. Correspondingly, more {100} facets will expose on the surface of larger PbX CQDs (Fig. 4b),[84] and present challenges to the related photovoltaic devices. (i) Research studies have revealed that the nonpolar {100} facets are self-passivated, leaving no sites for passivants. As a result, the unprotected {100} facets are susceptible to oxidation. (ii) The {100} facet consists of both cations and anions, which are easy to fuse with the {100} facet from another QD.[85–87] The fusion of CQDs can lead to an inhomogeneous energy landscape and bandtail states, which results in the loss of open-circuit voltage and decreased device performance.[17] Thus, the previously established surface-passivation strategies mainly toward the {111} facet will be no longer suitable for large size PbX CQDs. To obtain efficient IR CQD solar cells, new passivation methods have to be developed for large-size CQDs.

Infrared CQD solar cells were demonstrated in the early years. The traditional thiols were used as the surface ligand, showing PCEs typically less than 5%.[62,88,89] The ubiquitous fusion between the adjacent large CQDs during ligand exchange is considered as one of the critical issues limiting the performance of infrared CQD solar cells. To address this issue, Ip *et al.* pre-treated PbS CQDs with bromopropanethiol before solid-state ligand exchange, which avoided the fusion to some extent, and obtained a PCE of 7.3% and an IR-PCE of 0.8%.[90] The performance was further improved to 7.9% through surface passivation and device structure engineering.[91] However, device fabrication required a tedious LbL process. To avoid that, Kiani *et al.* first introduced an SPLE strategy to infrared solar cells and realized one-step film deposition,[92] while the PCE was only 3.5% (IR-PCE = 0.4%) due to the fusion and aggregation of CQDs. Then a pre-treatment with chloride passivation was introduced before the standard SPLE processing, which was able to preserve the integrity of IR CQDs in a solid film. As a result, a PCE of 6.57% and an IR-PCE of 0.76% were obtained.[93] It has been

Table 1 Solar cell performance based on small-size PbX CQD inks

	Device structures	V_{oc} (V)	J_{sc} (mA cm^{-2})	FF	PCE (%)	Year	Ref.
CQD ink passivation	ITO/TiO$_2$/PbS–(ArS, MPA)/MoO$_3$/Al	0.34	14.3	0.38	1.8	2013	31
	FTO/TiO$_2$/PbS–TG/MoO$_3$/Au/Ag	0.51	9.2	0.35	2.1	2013	30
	ITO/TiO/PbS–MAI/PbS–MPA/MoO$_3$/Au/Ag	0.50	23.0	0.53	6.1	2014	34
	ITO/ZnO/PbS–MAPbI$_3$/PbS–EDT/Au	0.61	21.8	0.68	8.9	2015	35
	ITO/ZnO/PbS–PbI$_2$/PbS–EDT/Au	0.65	24.8	0.63	10.1	2017	38
	ITO/ZnO/PbS–(PbI$_2$, PbBr$_2$)/PbS–EDT/Au	0.70	25.2	0.62	10.9	2017	41
	ITO/ZnO/PbS–(PbI$_2$, Pb(SCN)$_2$)/PbS–EDT/Au	0.60	31.5	0.59	11.2	2017	40
	ITO/ZnO/PbS–(PbI$_2$, PbBr$_2$)/PbS–EDT/Au	0.61	27.2	0.68	11.3	2017	17
	ITO/ZnO–Cl/PbS–(PbI$_2$, PbBr$_2$)/PbS–EDT/Au	0.63	28.4	0.65	11.63	2017	42
	ITO/InAs–MPA/PbS–PbI$_2$/PbS–EDT/Au	0.54	22.3	0.65	7.92	2018	68
	ITO/MZO/PbS–CsPbI$_3$/PbS–EDT/Au	0.64	24.5	0.67	10.5	2018	44
	ITO/ZnO/PbS–PbI$_2$/PbS–EDT/Au	0.66	28.8	0.57	11.0	2018	69
	ITO/ZnO/PbS–PbI$_2$/PbS–EDT/Au	0.65	29.0	0.64	12.0	2018	43
	ITO/ZnO/PbS (1.3eV)–(PbI$_2$, PbBr$_2$)/PbS (1.4eV)–(PbI$_2$, PbBr$_2$)/PbS–EDT/Au	0.63	28.8	0.68	12.3	2018	70
	ITO/ZnO/PbS–TBAI (ink)/PbS–EDT/Au	0.62	26.0	0.62	10.0	2019	71
	FTO/ZnO/PbS–PbI$_2$/PbS–EDT/Au	0.59	26.8	0.63	10.0	2019	72
	ITO/AZO/PbS–NH$_4$I/PbS–EDT/Au	0.65	26.6	0.66	11.4	2019	73
	ITO/ZnO/PbS–CsPbBr$_x$I$_{1-x}$/PbS–EDT/Au	0.64	28.9	0.68	12.6	2019	24
	ITO/ZnO/PbS–CsFAMAPbI$_3$/PbS–EDT/Au	0.59	28.9	0.66	11.3	2020	45
	ITO/ZnO/PbS–(PbI$_2$, PbBr$_2$)/PbS–EDT/Au	0.64	27.1	0.66	11.5	2020	74
	ITO/ZnO/PbS–PbI$_2$ (PbI$_2$, PbBr$_2$, KI)/PbS–EDT/Au	0.64	28.8	0.68	12.6	2020	75
	ITO/ZnO/PbS–FAPbBr$_3$(monolayer)/PbS–EDT/Au	0.65	30	0.71	13.8	2020	18
Bulk-homojunction	ITO/ZnO/PbS–PbI$_2$, PbS–TG/PbS–EDT/Au	0.62	26.8	0.64	10.4	2017	48
	ITO/ZnO/PbS–(PbI$_2$, PbBr$_2$), PbS–CTA/PbS–MA/Au	0.64	29.1	0.70	13.0	2020	76
	ITO/ZnO/PbS–(PbI$_2$, PbBr$_2$), PbS–CTA/PbS–EDT/Au	0.65	30.2	0.68	13.3	2020	49
Printable HTL	ITO/ZnO/PbS–PbI$_2$/polymer/MoO$_3$/Ag	0.57	27.9	0.60	9.6	2018	54
	ITO/ZnO/PbS–PbI$_2$ (ink)/PbS–MPA (ink)/Au	0.64	23.9	0.71	10.9	2018	77
	ITO/ZnO/PbS–PbI$_2$/polymer/MoO$_3$/Ag	0.60	28.3	0.65	11.2	2019	55
	ITO/ZnO/PbS–(PbI$_2$, PbBr$_2$)/SM–bridge–polymer/MoO$_3$/Ag	0.66	29.6	0.67	13.1	2019	58
	ITO/ZnO/PbS–PbI$_2$/Polymer/MoO$_3$/Ag	0.63	27.4	0.67	11.53	2020	56
	ITO/ZnO/PbS–PbI$_2$/organic BHJ/MoO$_3$/Ag	0.65	27.93	0.66	12.02	2020	57
PbSe	FTO/TiO$_2$/PbSe–PbI$_2$/Au	0.62	21.2	0.46	6.0	2018	78
	ITO/SnO$_2$/PCBM/PbSe–PbI$_2$/PbS–EDT/Au	0.54	28.4	0.68	10.4	2019	67
	ITO/ZnO/PbSe–PbI$_2$/PbS–EDT/Au	0.57	28.1	0.66	10.68	2019	79
	FTO/SnO$_2$/PbSe–PbI$_2$/PbS–EDT/Au	0.57	24.8	0.67	9.6	2020	80

Note: TG: 1-thioglycerol, ArS: 4-methylbenzenethiol, MPA: 3-mercaptopropionic acid, PEN: polyethylene naphthalate, AZO: Al-doped ZnO, MZO: Mg-doped ZnO, SM-bridge-polymer; small molecules-bridge-polymer, AI: ammonium iodide, MA: malonic acid.

observed that the standard SPLE for small-size PbS CQDs is insufficient to fully remove OA for large PbS CQDs.[94] Whereas, the addition of hydrohalic acid as additives during SPLE could more effectively complete the ligand exchange, leading to better passivation, greater QD packing density, and higher carrier mobility. As a result, a PCE of 7.9% and an IR-PCE of 0.86% were achieved.[94] To develop a specific passivation strategy for the {100} facets, the ammonium cation (NH$_4^+$) used in conventional SPLE was replaced with sodium ions, since sodium ions has appropriate size and high dissociation constant, beneficial for passivating the {100} facets (Fig. 4c).[95] By adopting the mixed lead halides (PbI$_2$, PbBr$_2$, and PbCl$_2$) as ligand precursors, an increased surface halide coverage was achieved. Consequently, improved halide passivation and charge transport were realized simultaneously, resulting in a PCE of 9.0% and an IR-PCE of 1.17%.[96] Xia et al. also reported a cation exchange strategy to achieve high monodisperse IR PbS CQDs from ZnS nanorods. The facets can be well passivated by chloride ions from the exchange precursors. The highest PCE and IR-PCE can reach 10% and 1.1%, respectively, using 0.95 eV bandgap PbS CQDs.[97]

Since single size CQD ink cannot fully utilize the solar energy within the 1100–1400 nm spectral region, the idea of using multi-bandgap CQD ink has been put forward successively. As reported by Sun et al.,[98] the mixing of two CQD inks with different QD sizes could not only increase the short-circuit current due to tailored optical response, but also improve the open-circuit voltage by inducing a larger quasi-Fermi level splitting, giving a PCE of 8.9% and IR-PCE of 0.95%. Kim et al. further developed this strategy by using a bilayer absorber architecture.[70] They used butylamine as the L-type ligand to render halide passivated PbS CQD inks with a larger bandgap soluble in non-polar solvents. The modified CQD ink could then be deposited onto the underneath CQD film consisting of smaller bandgap QDs. The bilayer structure with graded band-alignment could enhance the infrared absorption, improve the built-in potentials, and increase charge extraction in solar cells. As a result, the PCE and IR-PCE were improved to 9.5% and 1.1%, respectively. Recently, the CSM strategy reported in small CQDs was also employed in these large CQDs. Two IR CQD inks with different sizes were doped to p- and n-type to build BHJ structure. As a result, an IR-PCE of 1.37% was obtained.[99]
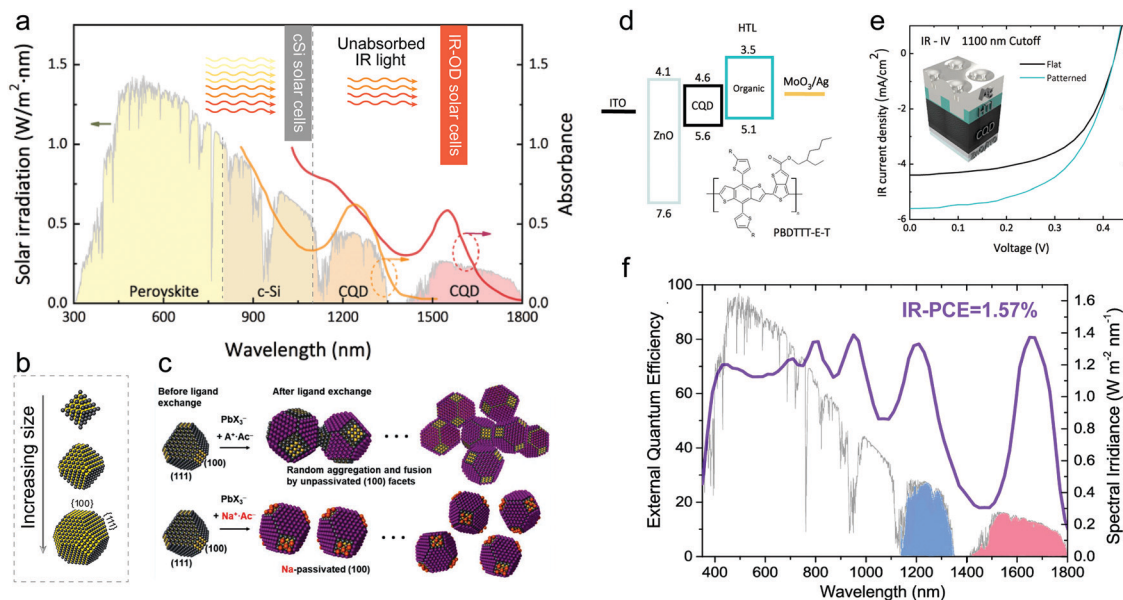
Fig. 4 (a) Illustration of IR CQD solar cells. The AM1.5G spectrum is shown as the black curve. Absorption onsets of perovskite and c-Si are indicated as dotted lines. Reprinted with permission from ref. 82. Copyright 2019, Wiley-VCH. (b) Size-dependent PbS QD crystal structures with larger size QDs exposing more {100} facets. Reprinted with permission from ref. 84. Copyright 2013, American Chemical Society. (c) Schematic illustrations of the conventional and facet-specific solution ligand exchanges for narrow-bandgap CQDs. Reprinted with permission from ref. 95. Copyright 2019, Wiley-VCH. (d) Energy level diagram of the hybrid CQD/organic device and chemical structure of the organic polymer used as HTL. (e) Representative J–V curves of IR CQD devices with (turquoise) and without (black) imprinting. The J–V was measured using the 1100 nm cutoff filter. The insert represents the device structure. Reprinted with permission from ref. 82. Copyright 2019, Wiley-VCH. (f) External quantum efficiency (EQE) of an IR CQD solar cell, with 80% value for both the first exciton peak at ∼1670 nm and the nearest Fabry–Perot resonance peak at ∼1210 nm. Reprinted with permission from ref. 83. Copyright 2020, American Chemical Society.

Nanostructured back reflector is another strategy to increase infrared light absorption in CQD solids. Baek *et al.* used polymer to replace the rigid PbS-EDT HTL. The nano-photonic structure was realized on this soft polymer layer through nanoimprinted lithography, which enhanced infrared light trapping, resulting in a high IR-PCE of 1.34% (Fig. 4d and e).[82] Note that the solar spectrum includes two IR regions, the first IR-region is between 1.1 eV (∼1.1 μm) and 0.9 eV (∼1.4 μm) and the second IR-region is between 0.9 eV (∼1.4 μm) and 0.7 eV (∼1.8 μm). Up to now, most IR CQD solar cells focus on the utilization of the first IR-region. Recently, Fan *et al.* developed an IR solar cell using PbS CQDs with the exciton peak at 1650 nm, targeting to utilize the second IR-region.[83] Interestingly, the closest Fabry–Perot resonance peak of the CQD film could cover the first IR-region as well. This IR solar cell with the thickest reported CQD film can achieve an external quantum efficiency of 80% in both IR-regions. As a result, the champion devices exhibited a J_{sc} of 38.9 mA cm^{-2}, currently the highest J_{sc} for all solution processed solar cells. This IR-PCE can reach 1.57%. The is also the highest IR-PCE so far.

The performances of IR CQD solar cells are listed in Table 2.

Table 2 Performance of IR solar cells based on PbS CQD inks

1st exciton peak	Solar illumination	V_{oc} (V)	J_{sc} (mA cm^{-2})	FF	PCE (%)	Year	Ref.
1300 nm	AM 1.5	0.38	18.1	0.54	3.7	2016	100
	1100 nm filter	0.29	2.4	0.58	0.4		
1180 nm	AM 1.5	0.54	22.4	0.54	6.5	2017	93
	1100 nm filter	0.44	2.7	0.62	0.7		
1148 nm	AM 1.5	0.53	26.1	0.60	8.0	2018	94
	1100 nm filter	0.43	3.2	0.67	0.9		
1150 nm, 1250 nm	AM 1.5	0.50	29.0	0.61	8.9	2018	98
	1100 nm filter	0.40	3.70	0.65	0.94		
1170 nm, 1250 nm	AM 1.5	0.47	37.4	0.54	9.5	2018	70
	1100 nm filter	0.41	4.1	0.64	1.1		
1142 nm	AM 1.5	0.53	26.1	58.1	8.1	2019	95
	1100 nm filter	0.43	3.2	0.65	0.9		
1180 nm	AM 1.5	0.47	28.3	0.54	7.2	2019	101
	Si cell filter	0.37	4.1	0.64	0.96		
1280 nm	AM 1.5	0.47	35.4	0.59	10.0	2019	97
	800 nm filter	0.44	15.7	0.61	4.2		
	1100 nm filter	0.39	4.3	0.64	1.1		
1150 nm	AM 1.5	0.56	31.4	0.46	8.0	2019	96
	1100 nm filter	0.47	4.4	0.59	1.2		
1188 nm	1100 nm filter	0.43	5.6	0.56	1.34	2019	82
1180 nm, 1250 nm	1100 nm filter	0.43	5.5	0.58	1.37	2020	99
1650 nm	AM 1.5	0.35	38.9	0.43	5.74	2020	83
	1100 nm filter	0.30	9.81	0.53	1.57		

3. PbS solar cells based on directly synthesized CQD inks

The SPLE processing indeed simplifies the device fabrication of PbX CQD solar cells. However, PbX CQDs have to be first synthesized with long-alkyl chain organic surface ligands and then be ligand-exchanged with shorter ligands (two-steps) to enable charge transport. Although several "green" and low-cost synthetic methods have been developed to synthesize PbX CQDs, nowadays, the most efficient photovoltaic devices still

rely on QDs synthesized from the typical hot-injection method by using the toxic and expensive hexamethyldisilathiane (TMS-S) as the sulfur precursor. The complicated precipitate/clean procedures also consume a large amount of solvents as well as labor (Fig. 5a). Jean *et al.* systematically analyzed the cost of fabrication of PbS CQD solar cells using a Monte Carlo model.[13] The typical synthesis step costs 10.6–59.2 \$ g^{-1}. And the SPLE process costs 6.3–8.7 \$ g^{-1}. Even by using the cheapest synthetic method, which has not yet been applied to photovoltaic devices, the preparation of PbS CQD inks (synthesis and SPLE) costs at least 16.9 \$ g^{-1} (0.24 \$ W^{-1}), which contributes 26% of the total cost (0.94 \$ W^{-1}) for PbS CQD solar cell modules. When using the most popular synthesis (PbAc$_2$ + TMS-S) and SPLE protocols, the cost could increase to as large as 35.3 \$ g^{-1} (0.50 \$ W^{-1}).[13] Furthermore, the added Pb content in solution-phase ligand exchange accounts for 46% of the total Pb produced during PbS solar cell fabrication, which requires extra cost for hazardous waste disposal.[71] It has been estimated that the commercial viability of PbS CQD solar cells could only be implemented when the cost of PbS CQD inks could be reduced to 5 \$ g^{-1}.[13] Therefore, the development of new low-cost synthetic methods is also crucial in addition to the improvement of device performance. Recently, Wang *et al.* developed a one-step method to directly synthesize semi-conducting PbS CQD inks. PbI$_2$ and *N,N*-diphenylthiourea (DPhTA) were used as the precursors for lead and sulfur respectively in DMF. The reaction was triggered by injecting butylamine to react with DPhTA and release HS$^-$, which works as the real active sulfur precursor. After purification, the PbS CQD inks can be well dispersed in DMF, and directly used for device preparation (Fig. 5b) without additional ligand exchange processing. More importantly, this reaction was conducted at room temperature and could be easily scaled up. A yield of 88 g CQD inks has been reported for one pot reaction in the lab (Fig. 5c). As a result, the cost of PbS CQD inks was calculated to be lower than 5.05 \$ g^{-1}, which reached the cost threshold estimated by Jean *et al.* (Fig. 5d).[13] Finally, the photovoltaic device based on these directly synthesized inks could reach 10.1%, showing potential for the future commercialization of CQD based optoelectronics.[12]

4. Large-area solar cells based on PbX CQD inks

Benefiting from the numerous innovations in PbX CQD inks, the advances of CQDs in solution processability have been translated into the fabrication of large-area solar cells. Recently, a high PCE of 10.3% has been demonstrated for CQD solar cells with an active area of 1.1 cm^2 by spin coating.[43] However, spin coating lacks compatibility with fast manufacturing techniques such as roll-to-roll printing. Fortunately, a densely packed crystalline CQD solid can be easily realized by a number of scalable deposition techniques, since it requires no control of crystallization during film deposition such as a perovskite solid, or fine phase separation like organics. We refer readers to a recent review for a detailed comparison of various coating methods.[22] In this chapter, we briefly introduce the upscaling coating methods and highlight their application for large area QD solar cells.

Meniscus-guided coating (MGC), where a meniscus is spontaneously formed as a result of interactions between the coating


Fig. 5 (a) General strategies for PbS CQD ink preparation, including two steps: (1) the synthesis of OA capped PbS CQDs (top). (2) SPLE process (bottom). Reprinted with permission from ref. 13. Copyright 2018, The Royal Society of Chemistry. (b) The procedure of one-step, direct synthesis of iodide capped PbS CQD inks. (c) Photos of a scaled-up 2L synthesis. 88 g of PbS CQD ink solid can be obtained in one-pot synthesis. The weight of the vial has been removed. (d) Cost of PbS CQD inks prepared with different methods according to real lab synthesis and Monte Carlo modeling. Reprinted with permission from ref. 12. Copyright 2019, Nature Publishing Group. The minimum cost protocol denotes the synthesis of OA capped PbS CQDs with PbCl$_2$ and thioacetamide as precursors (which has not yet been applied to photovoltaic devices) and the SPLE using PbI$_2$ according to ref. 38. The optimal protocol denotes the synthesis of OA capped PbS CQDs with PbAc$_2$ and TMS-S as precursors and the SPLE using PbI$_2$ + PbBr$_2$ + NH$_4$Ac according to ref. 17.

head and solvent, is one of the most promising techniques for the large-area production of solution-processed photoelectronic devices.[102] Except for nearly 99% usage of active materials, the intrinsic directionality of the coating process confers dense packing of colloidal solid, providing compatibility toward scalable manufacturing and flexible substrates.[103,104] Generally, the common MGC techniques include dip coating, convective assembly, doctor blading, and slot die coating. Dip-coating has been demonstrated as an effective method for control over CQD packing and superlattice assembly, which is capable of large area fabrication.[92,105,106] Due to the lengthy LbL dip-coating method, the studies of scalable MGC fabrication have been focused on the single-step deposition endowed by SPLE. Havid Aqoma *et al.* have demonstrated high-efficiency doctor-bladed CQD solar cells prepared by p- and n-type CQD inks, significantly simplifying the device fabrication process, achieving an efficiency of 10.01% (~8.6%) with an active area of 0.071 cm^2 (0.504 cm^2).[77] Meanwhile, Ahmad R. Kirmani *et al.* also reported n-type CQD ink based solar cells made by the same doctor blading technique with an efficiency of 11.0% (9.2%) with an active area of 0.1 cm^2 (1.1 cm^2) (Fig. 6a and b).[69] Besides, the capillary attractions between CQDs and the substrate during the convective assembly

process could promote the infiltration of CQDs into the ordered substrates such as ZnO nanorod arrays, forming a highly efficient ordered bulk heterojunction structure by a scalable manner.[107]

Other attempts toward the upscale manufacturing of CQD solar cells have been made, such as spray coating. The process involves the forcing of CQD solution through a nozzle, whereby sub-micron ordered aerosols are formed. Driven by the gas flows, the aerosol could be directed at the surface of a substrate, allowing patterns with millimeter-scale details and large-area manufacturing. An automated spray coating setup was demonstrated that could give substantial improvements of the CQD packing and device performance, confirmed by less inter-dot spacing and one order of magnitude higher elastic moduli compared with LbL spin-coated CQD solid.[108] However, tens of LbL cycles have to be conducted for each solar cell, leading to complications and material wastage for device fabrication. A simplified spray coating process with supersonic streams has been realized by using SPLE processed PbS CQD inks, whereas an unfavorable PCE of less than 4% was obtained, attributed to the poor ink colloidal stability and surface roughening of CQD solids.[109] This deficiency in film morphology can be overcome
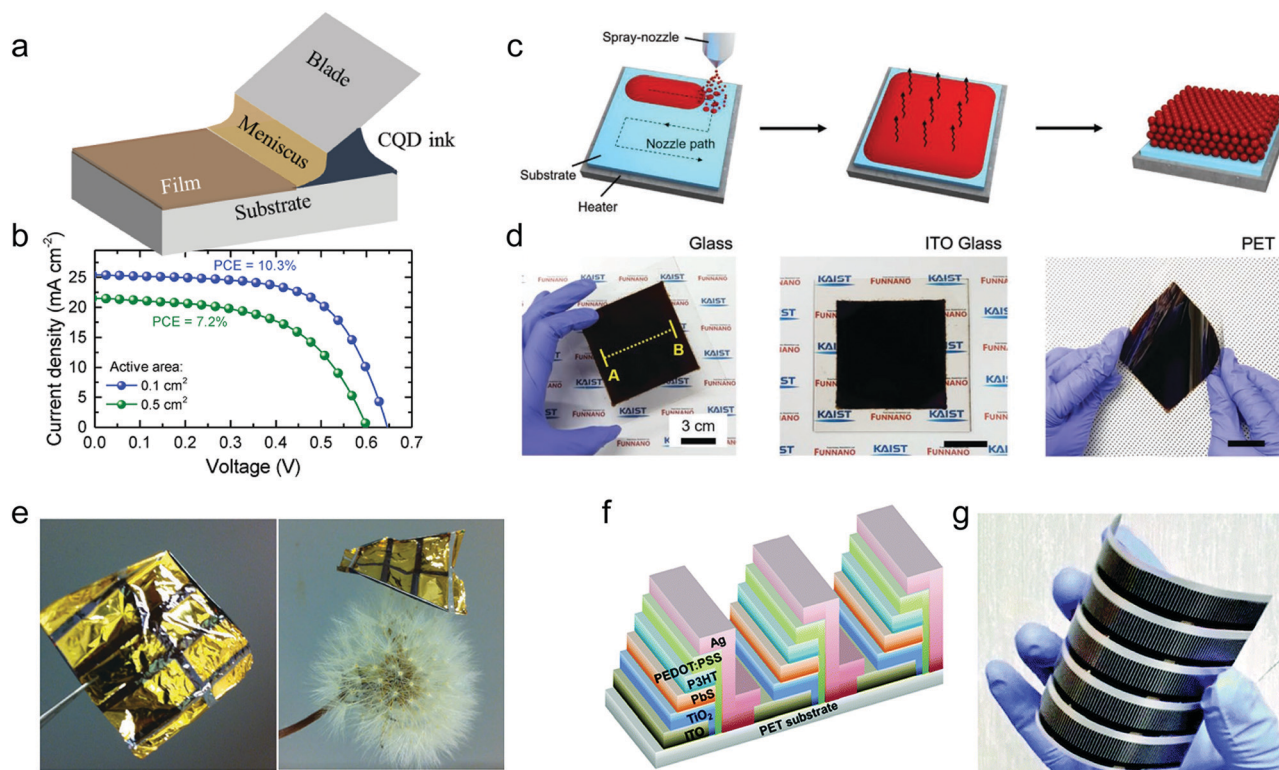
Fig. 6 (a) Schematic of the employed blade-coating setup. (b) *J*–*V* curves of 0.1 cm^2 (blue) and 0.5 cm^2 (green) active area blade-coated solar cells. Reprinted with permission from ref. 69. Copyright 2018, Wiley-VCH. (c) Scheme of the fabrication process of CQD films by using the spray-coating method. (d) Photograph of CQD films (10 cm × 10 cm) on a glass substrate, indium tin oxide (ITO) glass substrate, and polyethylene terephthalate (PET) substrate. Reprinted with permission from ref. 110. Copyright 2019, Wiley-VCH. (e) Photograph of the flexible PbS CQD solar cell. The size of the flexible substrate with six solar cells is ~2 × 2 cm^2. The flexible solar cell is placed on a dandelion without any deformation of the dandelion, illustrating its extremely lightweight feature. Reprinted with permission from ref. 112. Copyright 2018, The Royal Society of Chemistry. (f) Schematic diagram of the serial connection of PbS CQD solar cells. (g) Photograph of the PbS CQD solar modules on the flexible PET film with an active area of 30 cm^2, which was fabricated employing R2R printing. Reprinted with permission from ref. 113. Copyright 2015, The Royal Society of Chemistry.

Table 3 Summary of PbX CQD solar cells based on different coating technologies toward large-area fabrication

Active area (cm^2)	Deposition methods	CQD availability	Processing speed	Roll-to-roll compatibility	PCE (%)	Ref.
1.1	Spin coating	Extremely low	Slow	No	10.3	43
1.1	Spin coating	Extremely low	Slow	No	9.8	49
0.049	MGC-Dip-coating	Low	Slow	No	9.2	114
0.071	MGC-doctor blading	High	Fast	Yes	10.01	77
0.504	MGC-doctor blading	High	Fast	Yes	8.3	50
0.1	MGC-doctor blading	High	Fast	Yes	11.0	69
1.1	MGC-doctor blading	High	Fast	Yes	9.2	69
0.05	MGC-CA	High	Slow	Yes	9.92	107
0.049	Spray coating	Low	Slow	Yes	8.1	108
0.03	Spray coating	High	Fast	Yes	3.76	109
0.0314	Spray coating	High	Fast	Yes	8.1	110
30	Roll-to-roll	High	Fast	Yes	1.3	113

Note: CA: convective assembly.

by engineering the solute redistribution of CQD droplets on the substrate, where the CQD film formation is dominated by the movement of the contact line and the evaporation kinetics of the solvent. A large-area CQD film up to 100 cm^2 was spray-coated with a 3–7% thickness variation on different substrates. Resultantly, a notable high efficiency of 8.10% with an active area of 0.0314 cm^2 was achieved (Fig. 6c and d).[110]

The challenge of upscaling CQD based photovoltaics still lies in finding the optimal conditions that ensure both device efficiency and fast processing, which could further compress the cost into a commercial level. For solution-processed electronics possessing advances such as low-cost, fast deposition, and flexible applications, an ultimate setup could come to the roll-to-roll (R2R) coating techniques, where high-volume production is carried out in the form of a continuous roll of soft materials.[111] An ultra-flexible PbS CQD solar cell with a high power-per-weight output of 15.2 W g^{-1} was exhibited, revealing the compatibility of CQD based electronics with R2R and lightweight applications (Fig. 6e).[112] Furthermore, a PbS CQD solar module by the all-printing LbL process on a flexible substrate was demonstrated. The solar modules show a PCE of 1.3% with an active-area up to 30 cm^2, providing a promising reference for the production of CQD solar cells in a low-cost, large-area, and printable manner (Fig. 6f and g).[113] Nonetheless, the realization of fast film deposition and low material consumption in R2R encourages the single-step deposition of an active CQD layer by using SPLE or directly synthesized CQD inks, rather than complex LbL methods, whereas the control of ink colloidal stability and QD packing in large area CQD solids remains to be challenging. The management of inter-dot interaction in CQD inks that governs the long-range ordering of CQD packing and uniformity of large-area films during scalable deposition processing needs to be further studied. The summary information of PbX CQD solar cells toward large-area fabrication is listed in Table 3.

Nowadays, the development of large-area QD solar cells is still in the infant stage because an efficient device based on the QD inks has just been realized in the last several years. And the unsatisfactory colloid stability and high preparation cost of the QD inks have just been partly solved in the last two years. However, we believe that these initial results can accelerate the development of large-area QD solar cells in the near future.

5. Conclusions and perspectives

The past decade has witnessed the spectacular progress of PbX CQD solar cells. In particular, the recently developed PbX CQD inks boost the efficiency up to 13.8% with a simplified device fabrication process. Progress has been made on the way towards a theoretical efficiency of up to 45% in PbX CQD solar cells, originating from the advances of the MEG effect. More importantly, the superior stability of PbX CQDs among solution-processed photovoltaic materials suggests promising prospects for future commercialization. The recent success on efficient and low-cost CQD inks brings new insights into the development of PbX CQD electronics, which outperform the conventional LbL processing in the aspects of both photovoltaic performance and device processability. In general, the current advances in PbX CQDs make them ideal building blocks for printable large-area solar cells. Thus, we propose a few suggestions for future development alone in this direction:

(1) The primary focus of PbX CQD solar cells is still the improvement of device performance. Although the recent CQD ink engineering has promoted the device performance, the record PCE of PbX CQD solar cells (13.8%) still lags far behind that of the organic (17.4%) and perovskite (25.2%) solar cells.[115] The trap state-induced large V_{oc}-loss is the central limitation for device performance. The CQDs require more efficient passivation strategies to reduce these detrimental trap states. Recently, the use of a defect-tolerant perovskite material as a surface matrix on PbS CQDs is regarded as a promising direction.[24,33,43] The matrix thickness should be very pivotal to balance the inter-dot coupling and surface passivation. Too thick a shell layer will inevitably impede charge transport between the CQDs. Whereas, a too thin matrix cannot fully passivate the surface trap states. Meanwhile, the homogeneity of the matrix layer can affect the structural and energetic disorder of CQD films. Therefore, it requires sophisticated engineering of the matrix layer to achieve suitable thickness as well as homogeneity. The recently developed bulk-homojunction is another promising strategy to support efficient carrier collection in a thick CQD layer and to further improve device performance. To maximize the photovoltaic performance, the doping density of p- and n-type CQD inks needs to be finely adjusted. However, the doping density is basically restricted by the associated surface passivation

methods. Considering currently the very limited selection of efficient passivation methods for PbS CQDs, it is of significance to search for other approaches to engineer the CQD doping densities, such as heterovalent substitutional doping, which can decouple QD doping from surface passivation.[116]

(2) For printing mass fabrication, the long-term colloid stability of PbX CQD ink is crucial. Currently, the most popular protocol of PbS CQD ink relies on corrosive butylamine as the solvent. However, the CQDs tend to seriously aggregate in butylamine within one day and even decompose after long storage time.[117] Recently, several efforts have been made to improve the colloid stability. But it's still challenging to obtain efficient device performance using the aged CQD inks instead of fresh ones.[73,118] Furthermore, the fast printing deposition requires that the solvents have an appropriate boiling point and suitable viscosity *etc.*[117] Butylamine is no longer the optimum choice. Further work can be conducted to improve the ink colloid stability, and broaden the selection of ink solvents to achieve optimal printing conditions. To realize that, an in-depth understanding of the CQD surface configuration and ink chemistry is necessary, which, however, has not been fully uncovered yet. It is worth noting that the one-step directly synthesized PbS CQD ink demonstrates excellent ink stability in various solvents.

During the fabrication of the large-area devices, the control over film morphology is also of interest. Prior work has demonstrated that ordered CQD superlattice films exhibit improved charge transport compared to the disordered ones.[119] During spin coating, the CQD solution dries very fast with almost no possibility to form long-range ordered packing. Whereas, the solution drying process in MGC is intrinsically slower than that in spin-coating, which leaves enough time window for the CQDs to form a more ordered large-range superlattice. These different assembling features and their effect on the photovoltaic performance are valuable subjects in the research of larger-area CQD solar cells.

(3) Finally, we highlight the one-step directly synthesized CQD ink. The SPLE method has simplified the device fabrication, but still increased the material preparation cost. Moreover, in the current two-step protocol, both the CQD synthesis and SPLE process are difficult to scale up. The recently reported direct synthesis of PbS CQD ink could be an exciting avenue for large-scale manufacturing processes, considering its low cost (~ 5 \$ g^{-1}) and excellent colloidal stability. Previously, the initial CQD synthesis and post passivation were usually separated. In the direct synthesis of CQD inks regime, the *in situ* surface passivation can be realized during the initial CQD synthesis. It can provide opportunities to passivate the sites that are inaccessible in the traditional post passivation.[120,121] The realization of comprehensive surface passivation will definitely benefit the photovoltaic performance. Moreover, most efforts are focused on how to completely exchange the original OA ligand and avoid surface damage in the previous ligand exchange process. The material design (adjustment of composition, doping, *etc.*) has largely been neglected in previous studies. The direct synthesis of QD inks provides new

opportunities for material design, which can inspire innovation for CQD solar cells. The challenge of this infant method is the limited control on size and size distribution, which needs to be solved through a systematic study on the nucleation and growth process.

Conflicts of interest

There are no conflicts to declare.

Acknowledgements

References

1 O. Voznyy, B. R. Sutherland, A. H. Ip, D. Zhitomirsky and E. H. Sargent, *Nat. Rev. Mater.*, 2017, **2**, 17026.

2 Best Research Cell Efficiencies (NREL, accessed on 1 August 2020), https://www.nrel.gov/pv/cell-efficiency.html.

3 W. A. Dunlap-Shohl, Y. Zhou, N. P. Padture and D. B. Mitzi, *Chem. Rev.*, 2019, **119**, 3193–3295.

4 W. Nie, H. Tsai, R. Asadpour, J.-C. Blancon, A. J. Neukirch, G. Gupta, J. J. Crochet, M. Chhowalla, S. Tretiak and M. A. Alam, *Science*, 2015, **347**, 522–525.

5 Champion Photovoltaic Module Efficiency (NREL, accessed on 1 August 2020), https://www.nrel.gov/pv/module-efficiency.html.

6 A. J. Heeger, *Adv. Mater.*, 2014, **26**, 10–27.

7 J. Y. Woo, J. H. Ko, J. H. Song, K. Kim, H. Choi, Y. H. Kim, D. C. Lee and S. Jeong, *J. Am. Chem. Soc.*, 2014, **136**, 8883–8886.

8 C. H. Chuang, P. R. Brown, V. Bulovic and M. G. Bawendi, *Nat. Mater.*, 2014, **13**, 796–801.

9 S. Almosni, A. Delamarre, Z. Jehl, D. Suchet, L. Cojocaru, M. Giteau, B. Behaghel, A. Julian, C. Ibrahim, L. Tatry, H. Wang, T. Kubo, S. Uchida, H. Segawa, N. Miyashita, R. Tamaki, Y. Shoji, K. Yoshida, N. Ahsan, K. Watanabe, T. Inoue, M. Sugiyama, Y. Nakano, T. Hamamura, T. Toupance, C. Olivier, S. Chambon, L. Vignau, C. Geffroy, E. Cloutet, G. Hadziioannou, N. Cavassilas, P. Rale, A. Cattoni, S. Collin, F. Gibelli, M. Paire, L. Lombez, D. Aureau, M. Bouttemy, A. Etcheberry, Y. Okada and J. F. Guillemoles, *Sci. Technol. Adv. Mater.*, 2018, **19**, 336–369.

10 J. J. Choi, J. Luria, B.-R. Hyun, A. C. Bartnik, L. Sun, Y.-F. Lim, J. A. Marohn, F. W. Wise and T. Hanrath, *Nano Lett.*, 2010, **10**, 1805–1811.

11 J. Jasieniak, B. I. MacDonald, S. E. Watkins and P. Mulvaney, *Nano Lett.*, 2011, **11**, 2856–2864.

12 Y. Wang, Z. Liu, N. Huo, F. Li, M. Gu, X. Ling, Y. Zhang, K. Lu, L. Han, H. Fang, A. G. Shulga, Y. Xue, S. Zhou, F. Yang, X. Tang, J. Zheng, M. Antonietta Loi, G. Konstantatos and W. Ma, *Nat. Commun.*, 2019, **10**, 5136.

13 J. Jean, J. Xiao, R. Nick, N. Moody, M. Nasilowski, M. Bawendi and V. Bulović, *Energy Environ. Sci.*, 2018, **11**, 2295–2305.

14 T. P. Osedach, T. L. Andrew and V. Bulović, *Energy Environ. Sci.*, 2013, **6**, 711–718.

15 R. Wang, Y. Shang, P. Kanjanaboos, W. Zhou, Z. Ning and E. H. Sargent, *Energy Environ. Sci.*, 2016, **9**, 1130–1143.

16 K. Lu, X. Meng, Z. Liu, J. Chen, Y. Wang, Y. Zhang, X. Zhang, E. Sarnello, G. Shi, R. P. Patil, W. Deng, S. Zhou, M. Gu, Y. Zhong, S. Jeong, X. W. Gu, T. Li, X. Ye and W. Ma, *Cell Rep. Phys. Sci.*, 2020, **1**, 100183.

17 M. Liu, O. Voznyy, R. Sabatini, F. P. Garcia de Arquer, R. Munir, A. H. Balawi, X. Lan, F. Fan, G. Walters, A. R. Kirmani, S. Hoogland, F. Laquai, A. Amassian and E. H. Sargent, *Nat. Mater.*, 2017, **16**, 258–263.

18 B. Sun, A. Johnston, C. Xu, M. Wei, Z. Huang, Z. Jiang, H. Zhou, Y. Gao, Y. Dong, O. Ouellette, X. Zheng, J. Liu, M.-J. Choi, Y. Gao, S.-W. Baek, F. Laquai, O. M. Bakr, D. Ban, O. Voznyy, F. P. García de Arquer and E. H. Sargent, *Joule*, 2020, **4**, 1542–1556.

19 K. Lu, Y. Wang, Z. Liu, L. Han, G. Shi, H. Fang, J. Chen, X. Ye, S. Chen, F. Yang, A. G. Shulga, T. Wu, M. Gu, S. Zhou, J. Fan, M. A. Loi and W. Ma, *Adv. Mater.*, 2018, **30**, 1707572.

20 G. H. Carey, A. L. Abdelhady, Z. Ning, S. M. Thon, O. M. Bakr and E. H. Sargent, *Chem. Rev.*, 2015, **115**, 12732–12763.

21 Z. Liu, J. Yuan, S. A. Hawks, G. Shi, S.-T. Lee and W. Ma, *Sol. RRL*, 2017, **1**, 1600021.

22 H. Lee, H. J. Song, M. Shim and C. Lee, *Energy Environ. Sci.*, 2020, **13**, 404–431.

23 M. C. Weidman, M. E. Beck, R. S. Hoffman, F. Prins and W. A. Tisdale, *ACS Nano*, 2014, **8**, 6363–6371.

24 M. Liu, Y. Chen, C. S. Tan, R. Quintero-Bermudez, A. H. Proppe, R. Munir, H. Tan, O. Voznyy, B. Scheffel, G. Walters, A. P. T. Kam, B. Sun, M. J. Choi, S. Hoogland, A. Amassian, S. O. Kelley, F. P. Garcia de Arquer and E. H. Sargent, *Nature*, 2019, **570**, 96–101.

25 E. H. Sargent, *Nat. Photonics*, 2012, **6**, 133–135.

26 B. Sun, E. Marx and N. C. Greenham, *Nano Lett.*, 2003, **3**, 961–963.

27 I. Lokteva, N. Radychev, F. Witt, H. Borchert, J. Parisi and J. Kolny-Olesiak, *J. Phys. Chem. C*, 2010, **114**, 12784–12791.

28 K. W. Johnston, A. G. Pattantyus-Abraham, J. P. Clifford, S. H. Myrskog, D. D. MacNeil, L. Levina and E. H. Sargent, *Appl. Phys. Lett.*, 2008, **92**, 151115.

29 S. A. Mcdonald, G. Konstantatos, S. Zhang, P. W. Cyr, E. J. D. Klem, L. Levina and E. H. Sargent, *Nat. Mater.*, 2005, **4**, 138–142.

30 A. Fischer, L. Rollny, J. Pan, G. H. Carey, S. M. Thon, S. Hoogland, O. Voznyy, D. Zhitomirsky, J. Y. Kim, O. M. Bakr and E. H. Sargent, *Adv. Mater.*, 2013, **25**, 5742–5749.

31 C. Giansante, L. Carbone, C. Giannini, D. Altamura, Z. Ameer, G. Maruccio, A. Loiudice, M. R. Belviso, P. D. Cozzoli, A. Rizzo and G. Gigli, *J. Phys. Chem. C*, 2013, **117**, 13305–13317.

32 D. N. Dirin, S. Dreyfuss, M. I. Bodnarchuk, G. Nedelcu, P. Papagiorgis, G. Itskos and M. V. Kovalenko, *J. Am. Chem. Soc.*, 2014, **136**, 6550–6553.

33 Z. Ning, X. Gong, R. Comin, G. Walters, F. Fan, O. Voznyy, E. Yassitepe, A. Buin, S. Hoogland and E. H. Sargent, *Nature*, 2015, **523**, 324–328.

34 Z. Ning, H. Dong, Q. Zhang, O. Voznyy and E. H. Sargent, *ACS Nano*, 2014, **8**, 10321–10327.

35 Z. Yang, A. Janmohamed, X. Lan, F. P. Garcia de Arquer, O. Voznyy, E. Yassitepe, G. H. Kim, Z. Ning, X. Gong, R. Comin and E. H. Sargent, *Nano Lett.*, 2015, **15**, 7539–7543.

36 S. Kim, J. Noh, H. Choi, H. Ha, J. H. Song, H. C. Shim, J. Jang, M. C. Beard and S. Jeong, *J. Phys. Chem. Lett.*, 2014, **5**, 4002–4007.

37 J. Y. Kim, V. Adinolfi, B. R. Sutherland, O. Voznyy, S. J. Kwon, T. W. Kim, J. Kim, H. Ihee, K. Kemp, M. Adachi, M. Yuan, I. Kramer, D. Zhitomirsky, S. Hoogland and E. H. Sargent, *Nat. Commun.*, 2015, **6**, 7772.

38 H. Aqoma, M. Al Mubarok, W. T. Hadmojo, E. H. Lee, T. W. Kim, T. K. Ahn, S. H. Oh and S. Y. Jang, *Adv. Mater.*, 2017, **29**, 1605756.

39 X. Zhang, U. B. Cappel, D. Jia, Q. Zhou, J. Du, T. Sloboda, S. Svanström, F. O. L. Johansson, A. Lindblad, E. Giangrisostomi, R. Ovsyannikov, J. Liu, H. Rensmo, J. M. Gardner and E. M. J. Johansson, *Chem. Mater.*, 2019, **31**, 4081–4091.

40 B. Sun, O. Voznyy, H. Tan, P. Stadler, M. Liu, G. Walters, A. H. Proppe, M. Liu, J. Fan, T. Zhuang, J. Li, M. Wei, J. Xu, Y. Kim, S. Hoogland and E. H. Sargent, *Adv. Mater.*, 2017, **29**, 1700749.

41 J. W. Jo, Y. Kim, J. Choi, F. P. G. de Arquer, G. Walters, B. Sun, O. Ouellette, J. Kim, A. H. Proppe, R. Quintero-Bermudez, J. Fan, J. Xu, C. S. Tan, O. Voznyy and E. H. Sargent, *Adv. Mater.*, 2017, **29**, 1703627.

42 J. Choi, Y. Kim, J. W. Jo, J. Kim, B. Sun, G. Walters, F. P. García de Arquer, R. Quintero-Bermudez, Y. Li, C. S. Tan, L. N. Quan, A. P. T. Kam, S. Hoogland, Z. Lu, O. Voznyy and E. H. Sargent, *Adv. Mater.*, 2017, 1702350.

43 J. Xu, O. Voznyy, M. Liu, A. R. Kirmani, G. Walters, R. Munir, M. Abdelsamie, A. H. Proppe, A. Sarkar, F. P. Garcia de Arquer, M. Wei, B. Sun, M. Liu, O. Ouellette, R. Quintero-Bermudez, J. Li, J. Fan, L. Quan, P. Todorovic, H. Tan, S. Hoogland, S. O. Kelley, M. Stefik, A. Amassian and E. H. Sargent, *Nat. Nanotechnol.*, 2018, **13**, 456–462.

44 X. Zhang, J. Zhang, D. Phuyal, J. Du, L. Tian, V. Oberg, M. Johansson, U. Cappel, O. Karis, J. Liu, H. Rensmo, G. Boschloo and E. Johansson, *Adv. Energy Mater.*, 2018, **8**, 1702049.

45 M. Albaladejo-Siguan, D. Becker-Koch, A. D. Taylor, Q. Sun, V. Lami, P. G. Oppenheimer, F. Paulus and Y. Vaynzof, *ACS Nano*, 2020, **14**, 384–393.

46 J. Tang and E. H. Sargent, *Adv. Mater.*, 2011, **23**, 12–29.

47 D. Zhitomirsky, O. Voznyy, L. Levina, S. Hoogland, K. W. Kemp, A. H. Ip, S. M. Thon and E. H. Sargent, *Nat. Commun.*, 2014, **5**, 3803.

48 Z. Yang, J. Z. Fan, A. H. Proppe, F. P. G. Arquer, D. Rossouw, O. Voznyy, X. Lan, M. Liu, G. Walters, R. Quintero-Bermudez, B. Sun, S. Hoogland, G. A. Botton, S. O. Kelley and E. H. Sargent, *Nat. Commun.*, 2017, **8**, 1325.

49 M. J. Choi, F. P. Garcia de Arquer, A. H. Proppe, A. Seifitokaldani, J. Choi, J. Kim, S. W. Baek, M. Liu, B. Sun, M. Biondi, B. Scheffel, G. Walters, D. H. Nam, J. W. Jo, O. Ouellette, O. Voznyy, S. Hoogland, S. O. Kelley, Y. S. Jung and E. H. Sargent, *Nat. Commun.*, 2020, **11**, 103.

50 H. Aqoma and S.-Y. Jang, *Energy Environ. Sci.*, 2018, **11**, 1603–1609.

51 Z. Liu, Y. Sun, J. Yuan, H. Wei, X. Huang, L. Han, W. Wang, H. Wang and W. Ma, *Adv. Mater.*, 2013, **25**, 5772–5778.

52 Y. X. Sun, Z. K. Liu, J. Y. Yuan, J. M. Chen, Y. Zhou, X. D. Huang and W. L. Ma, *Org. Electron.*, 2015, **24**, 263–271.

53 K. Lu, Y. Wang, J. Yuan, Z. Cui, G. Shi, S. Shi, L. Han, S. Chen, Y. Zhang, X. Ling, Z. Liu, L. Chi, J. Fan and W. Ma, *J. Mater. Chem. A*, 2017, **5**, 23960–23966.

54 H. Aqoma, M. Al Mubarok, W. Lee, W. T. Hadmojo, C. Park, T. K. Ahn, D. Y. Ryu and S. Y. Jang, *Adv. Energy Mater.*, 2018, **8**, 1800572.

55 Y. Xue, F. Yang, J. Y. Yuan, Y. N. Zhang, M. F. Gu, Y. L. Xu, X. F. Ling, Y. Wang, F. C. Li, T. S. Zhai, J. N. Li, C. H. Cui, Y. W. Chen and W. L. Ma, *ACS Energy Lett.*, 2019, **4**, 2850–2858.

56 M. A. Mubarok, H. Aqoma, F. T. A. Wibowo, W. Lee, H. M. Kim, D. Y. Ryu, J. W. Jeon and S. Y. Jang, *Adv. Energy Mater.*, 2020, **10**, 2070035.

57 Y. N. Zhang, Y. Y. Kan, K. Gao, M. F. Gu, Y. Shi, X. L. Zhang, Y. Xue, X. N. Zhang, Z. K. Liu, Y. Zhang, J. Y. Yuan, W. L. Ma and A. K. Y. Jen, *ACS Energy Lett.*, 2020, **5**, 2335–2342.

58 S.-W. Baek, S. Jun, B. Kim, A. H. Proppe, O. Ouellette, O. Voznyy, C. Kim, J. Kim, G. Walters, J. H. Song, S. Jeong, H. R. Byun, M. S. Jeong, S. Hoogland, F. P. García de Arquer, S. O. Kelley, J.-Y. Lee and E. H. Sargent, *Nat. Energy*, 2019, **4**, 969–976.

59 F. W. Wise, *Acc. Chem. Res.*, 2000, **33**, 773–780.

60 M. C. Beard, J. M. Luther, O. E. Semonin and A. J. Nozik, *Acc. Chem. Res.*, 2013, **46**, 1252–1260.

61 L. A. Padilha, J. T. Stewart, R. L. Sandberg, W. K. Bae, W. K. Koh, J. M. Pietryga and V. I. Klimov, *Acc. Chem. Res.*, 2013, **46**, 1261–1269.

62 O. E. Semonin, J. M. Luther, S. Choi, H.-Y. Chen, J. Gao, A. J. Nozik and M. C. Beard, *Science*, 2011, **334**, 1530–1533.

63 J. Zhang, J. Gao, C. P. Church, E. M. Miller, J. M. Luther, V. I. Klimov and M. C. Beard, *Nano Lett.*, 2014, **14**, 6010–6015.

64 S. Kim, A. R. Marshall, D. M. Kroupa, E. M. Miller, J. M. Luther, S. Jeong and M. C. Beard, *ACS Nano*, 2015, **9**, 8157–8164.

65 L. Hu, Z. Zhang, R. J. Patterson, S. B. Shivarudraiah, Z. Zhou, M. Ng, S. Huang and J. E. Halpert, *Sol. RRL*, 2018, **2**, 1800234.

66 W. Ahmad, J. He, Z. Liu, K. Xu, Z. Chen, X. Yang, D. Li, Y. Xia, J. Zhang and C. Chen, *Adv. Mater.*, 2019, **31**, e1900593.

67 L. Hu, X. Geng, S. Singh, J. Shi, Y. Hu, S. Li, X. Guan, T. He, X. Li, Z. Cheng, R. Patterson, S. Huang and T. Wu, *Nano Energy*, 2019, **64**, 103922.

68 J. H. Song, H. Choi, H. T. Pham and S. Jeong, *Nat. Commun.*, 2018, **9**, 4267.

69 A. R. Kirmani, A. D. Sheikh, M. R. Niazi, M. A. Haque, M. Liu, F. P. G. de Arquer, J. Xu, B. Sun, O. Voznyy, N. Gasparini, D. Baran, T. Wu, E. H. Sargent and A. Amassian, *Adv. Mater.*, 2018, **30**, 1801661.

70 J. Kim, O. Ouellette, O. Voznyy, M. Wei, J. Choi, M. J. Choi, J. W. Jo, S. W. Baek, J. Fan, M. I. Saidaminov, B. Sun, P. Li, D. H. Nam, S. Hoogland, Z. H. Lu, F. P. Garcia de Arquer and E. H. Sargent, *Adv. Mater.*, 2018, 1803830.

71 N. Moody, D. Yoon, A. Johnson, E. Wassweiler, M. Nasilowski, V. Bulovic and M. G. Bawendi, *Adv. Sustainable Syst.*, 2019, **3**, 1900061.

72 L. Wang, Y. Wang, Y. Jia, X. Liu, T. Liu, T. Fu, J. Li, B. Weng, X. Zhang and Y. Liu, *J. Phys. Chem. C*, 2019, **123**, 30137–30144.

73 D. Jia, J. Chen, S. Zheng, D. Phuyal, M. Yu, L. Tian, J. Liu, O. Karis, H. Rensmo, E. M. J. Johansson and X. Zhang, *Adv. Energy Mater.*, 2019, **9**, 1902809.

74 Y. Xia, W. Chen, P. Zhang, S. Liu, K. Wang, X. Yang, H. Tang, L. Lian, J. He, X. Liu, G. Liang, M. Tan, L. Gao, H. Liu, H. Song, D. Zhang, J. Gao, K. Wang, X. Lan, X. Zhang, P. Müller-Buschbaum, J. Tang and J. Zhang, *Adv. Funct. Mater.*, 2020, **30**, 2000594.

75 J. Choi, M. J. Choi, J. Kim, F. Dinic, P. Todorovic, B. Sun, M. Wei, S. W. Baek, S. Hoogland, F. P. Garcia de Arquer, O. Voznyy and E. H. Sargent, *Adv. Mater.*, 2020, **32**, 1906497.

76 M. Biondi, M. J. Choi, O. Ouellette, S. W. Baek, P. Todorovic, B. Sun, S. Lee, M. Wei, P. Li, A. R. Kirmani, L. K. Sagar, L. J. Richter, S. Hoogland, Z. H. Lu, F. P. Garcia de Arquer and E. H. Sargent, *Adv. Mater.*, 2020, **32**, 1906199.

77 H. Aqoma and S.-Y. Jang, *Energy Environ. Sci.*, 2018, **11**, 1603–1609.

78 Y. Zhang, G. Wu, C. Ding, F. Liu, Y. Yao, Y. Zhou, C. Wu, N. Nakazawa, Q. Huang, T. Toyoda, R. Wang, S. Hayase, Z. Zou and Q. Shen, *J. Phys. Chem. Lett.*, 2018, **9**, 3598–3603.

79 W. Ahmad, J. He, Z. Liu, K. Xu, Z. Chen, X. Yang, D. Li, Y. Xia, J. Zhang and C. Chen, *Adv. Mater.*, 2019, 1900593.

80 M. Zhu, X. Liu, S. Liu, C. Chen, J. He, W. Liu, J. Yang, L. Gao, G. Niu, J. Tang and J. Zhang, *ACS Appl. Mater. Interfaces*, 2020, **12**, 2566–2571.

81 J. M. Pietryga, R. D. Schaller, D. Werder, M. H. Stewart, V. I. Klimov and J. A. Hollingsworth, *J. Am. Chem. Soc.*, 2004, **126**, 11752–11753.

82 S. W. Baek, P. Molet, M. J. Choi, M. Biondi, O. Ouellette, J. Fan, S. Hoogland, F. P. Garcia de Arquer, A. Mihi and E. H. Sargent, *Adv. Mater.*, 2019, **31**, 1901745.

83 J. Z. Fan, M. Vafaie, K. Bertens, M. Sytnyk, J. M. Pina, L. K. Sagar, O. Ouellette, A. H. Proppe, A. S. Rasouli, Y. Gao, S. W. Baek, B. Chen, F. Laquai, S. Hoogland, F. P. G. Arquer, W. Heiss and E. H. Sargent, *Nano Lett.*, 2020, **20**, 5284–5291.

84 H. Choi, J. H. Ko, Y. H. Kim and S. Jeong, *J. Am. Chem. Soc.*, 2013, **135**, 5278–5281.

85 B. K. Hughes, J. L. Blackburn, D. Kroupa, A. Shabaev, S. C. Erwin, A. L. Efros, A. J. Nozik, J. M. Luther and M. C. Beard, *J. Am. Chem. Soc.*, 2014, **136**, 4670–4679.

86 R. H. Gilmore, Y. Liu, W. Shcherbakov-Wu, N. S. Dahod, E. M. Y. Lee, M. C. Weidman, H. Li, J. Jean, V. Bulović, A. P. Willard, J. C. Grossman and W. A. Tisdale, *Matter*, 2019, **1**, 250–265.

87 J. C. Ondry, M. R. Hauwiller and A. P. Alivisatos, *ACS Nano*, 2018, **12**, 3178–3189.

88 J. M. Luther, M. Law, M. C. Beard, Q. Song, M. O. Reese, R. J. Ellingson and A. J. Nozik, *Nano Lett.*, 2008, **8**, 3488–3492.

89 E. J. D. Klem, D. D. MacNeil, P. W. Cyr, L. Levina and E. H. Sargent, *Appl. Phys. Lett.*, 2007, **90**, 183113.

90 A. H. Ip, A. Kiani, I. J. Kramer, O. Voznyy, H. F. Movahed, L. Levina, M. M. Adachi, S. Hoogland and E. H. Sargent, *ACS Nano*, 2015, **9**, 8833–8842.

91 Y. Bi, S. Pradhan, S. Gupta, M. Z. Akgul, A. Stavrinadis and G. Konstantatos, *Adv. Mater.*, 2018, **30**, 1704928.

92 A. Kiani, B. R. Sutherland, Y. Kim, O. Ouellette, L. Levina, G. Walters, C. T. Dinh, M. X. Liu, O. Voznyy, X. Z. Lan, A. J. Labelle, A. H. Ip, A. Proppe, G. H. Ahmed, O. F. Mohammed, S. Hoogland and E. H. Sargent, *Appl. Phys. Lett.*, 2016, **109**, 183105.

93 J. Z. Fan, M. Liu, O. Voznyy, B. Sun, L. Levina, R. Quintero-Bermudez, M. Liu, O. Ouellette, F. P. Garcia de Arquer, S. Hoogland and E. H. Sargent, *ACS Appl. Mater. Interfaces*, 2017, **9**, 37536–37541.

94 J. W. Jo, J. Choi, F. P. Garcia de Arquer, A. Seifitokaldani, B. Sun, Y. Kim, H. Ahn, J. Fan, R. Quintero-Bermudez, J. Kim, M. J. Choi, S. W. Baek, A. H. Proppe, G. Walters, D. H. Nam, S. Kelley, S. Hoogland, O. Voznyy and E. H. Sargent, *Nano Lett.*, 2018, **18**, 4417–4423.

95 Y. Kim, F. Che, J. W. Jo, J. Choi, F. P. Garcia de Arquer, O. Voznyy, B. Sun, J. Kim, M. J. Choi, R. Quintero-Bermudez, F. Fan, C. S. Tan, E. Bladt, G. Walters, A. H. Proppe, C. Zou, H. Yuan, S. Bals, J. Hofkens, M. B. J. Roeffaers, S. Hoogland and E. H. Sargent, *Adv. Mater.*, 2019, 1805580.

96 J. Z. Fan, N. T. Andersen, M. Biondi, P. Todorovic, B. Sun, O. Ouellette, J. Abed, L. K. Sagar, M. J. Choi, S. Hoogland, F. P. G. de Arquer and E. H. Sargent, *Adv. Mater.*, 2019, **31**, 1904304.

97 Y. Xia, S. Liu, K. Wang, X. Yang, L. Lian, Z. Zhang, J. He, G. Liang, S. Wang, M. Tan, H. Song, D. Zhang, J. Gao, J. Tang, M. C. Beard and J. Zhang, *Adv. Funct. Mater.*, 2019, **30**, 1907379.

98 B. Sun, O. Ouellette, F. P. Garcia de Arquer, O. Voznyy, Y. Kim, M. Wei, A. H. Proppe, M. I. Saidaminov, J. Xu, M. Liu, P. Li, J. Z. Fan, J. W. Jo, H. Tan, F. Tan, S. Hoogland, Z. H. Lu, S. O. Kelley and E. H. Sargent, *Nat. Commun.*, 2018, **9**, 4003.

99 M. J. Choi, S. W. Baek, S. Lee, M. Biondi, C. Zheng, P. Todorovic, P. C. Li, S. Hoogland, Z. H. Lu, F. P. G. de Arquer and E. H. Sargent, *Adv. Sci.*, 2020, **7**, 2000894.

100 A. Kiani, B. R. Sutherland, Y. Kim, O. Ouellette, L. Levina, G. Walters, C.-T. Dinh, M. Liu, O. Voznyy, X. Lan, A. J. Labelle, A. H. Ip, A. Proppe, G. H. Ahmed, O. F. Mohammed, S. Hoogland and E. H. Sargent, *Appl. Phys. Lett.*, 2016, **109**, 183105.

101 M. Liu, F. Che, B. Sun, O. Voznyy, A. Proppe, R. Munir, M. Wei, R. Quintero-Bermudez, L. Hu, S. Hoogland, A. Mandelis, A. Amassian, S. O. Kelley, F. P. García de Arquer and E. H. Sargent, *ACS Energy Lett.*, 2019, **4**, 1225–1230.

102 X. Gu, L. Shaw, K. Gu, M. F. Toney and Z. Bao, *Nat. Commun.*, 2018, **9**, 534.

103 P. Kumnorkaew, A. L. Weldon and J. F. Gilchrist, *Langmuir*, 2010, **26**, 2401–2405.

104 T. Muangnapoh, A. L. Weldon and J. F. Gilchrist, *Appl. Phys. Lett.*, 2013, **103**, 181603.

105 J. M. Luther, M. Law, M. C. Beard, Q. Song, M. O. Reese, R. J. Ellingson and A. J. Nozik, *Nano Lett.*, 2008, **8**, 3488–3492.

106 J. M. Luther, M. Law, Q. Song, C. L. Perkins, M. C. Beard and A. J. Nozik, *ACS Nano*, 2008, **2**, 271–280.

107 G. Shi, A. Kaewprajak, X. Ling, A. Hayakawa, S. Zhou, B. Song, Y. Kang, T. Hayashi, M. E. Altun, M. Nakaya, Z. Liu, H. Wang, T. Sagawa and W. Ma, *ACS Energy Lett.*, 2019, **4**, 960–967.

108 I. J. Kramer, J. C. Minor, G. Moreno-Bautista, L. Rollny, P. Kanjanaboos, D. Kopilovic, S. M. Thon, G. H. Carey, K. W. Chou, D. Zhitomirsky, A. Amassian and E. H. Sargent, *Adv. Mater.*, 2015, **27**, 116–121.

109 H. Choi, J. G. Lee, X. D. Mai, M. C. Beard, S. S. Yoon and S. Jeong, *Sci. Rep.*, 2017, **7**, 622.

110 M. J. Choi, Y. Kim, H. Lim, E. Alarousu, A. Adhikari, B. S. Shaheen, Y. H. Kim, O. F. Mohammed, E. H. Sargent, J. Y. Kim and Y. S. Jung, *Adv. Mater.*, 2019, 1805886.

111 F. C. Krebs, *Sol. Energy Mater. Sol. Cells*, 2009, **93**, 394–412.

112 X. Zhang, V. A. Öberg, J. Du, J. Liu and E. M. J. Johansson, *Energy Environ. Sci.*, 2018, **11**, 354–364.

113 J. Jang, H. C. Shim, Y. Ju, J. H. Song, H. An, J. S. Yu, S. W. Kwak, T. M. Lee, I. Kim and S. Jeong, *Nanoscale*, 2015, **7**, 8829–8834.

114 A. J. Labelle, S. M. Thon, S. Masala, M. M. Adachi, H. Dong, M. Farahani, A. H. Ip, A. Fratalocchi and E. H. Sargent, *Nano Lett.*, 2015, **15**, 1101–1108.

115 H. Wang, T. Kubo, J. Nakazaki and H. Segawa, *ACS Energy Lett.*, 2017, **2**, 2110–2117.

116 A. Stavrinadis, A. K. Rath, F. P. de Arquer, S. L. Diedenhofen, C. Magen, L. Martinez, D. So and G. Konstantatos, *Nat. Commun.*, 2013, **4**, 2981.

117 R. Sliz, M. Lejay, J. Z. Fan, M. J. Choi, S. Kinge, S. Hoogland, T. Fabritius, F. P. Garcia de Arquer and E. H. Sargent, *ACS Nano*, 2019, **13**, 11988–11995.

118 M. Gu, Y. Wang, F. Yang, K. Lu, Y. Xue, T. Wu, H. Fang, S. Zhou, Y. Zhang, X. Ling, Y. Xu, F. Li, J. Yuan, M. A. Loi, Z. Liu and W. Ma, *J. Mater. Chem. A*, 2019, **7**, 15951–15959.

119 A. Dong, Y. Jiao and D. J. Milliron, *ACS Nano*, 2013, **7**, 10978–10984.

120 Y. Wang, K. Lu, L. Han, Z. Liu, G. Shi, H. Fang, S. Chen, T. Wu, F. Yang, M. Gu, S. Zhou, X. Ling, X. Tang, J. Zheng, M. A. Loi and W. Ma, *Adv. Mater.*, 2018, **30**, 1704871.

121 J. Zhang, J. Gao, E. M. Miller, J. M. Luther and M. C. Beard, *ACS Nano*, 2014, **8**, 614–622.